Peer-reviewed version available at *Nanomaterials* **2019**, *9*, 1628; doi:10.3390/nano9111628

Effect of heterointerface on NO_2 sensing properties of in-situ formed TiO_2 QDs-decorated NiO nanosheets

Congyi Wu,[ab] *Jian Zhang,*[a] *Xiaoxia Wang,*[a] *Changsheng Xie,*[a] *Songxin Shi,**[b] *and Dawen Zeng,**[ac]

[a.] State Key Laboratory of Material Processing and Die & Mould Technology, School of Materials Science and Engineering, Huazhong University of Science and Technology (HUST), Wuhan 430074, P. R. China

[b.] National Engineering Research Center of Manufacturing Equipment Digitization, HUST, No. 1037, Luoyu Road, Wuhan 430074, China

[c.] Hubei Collaborative Innovation Center for Advanced Organic Chemical Materials, Hubei University, Wuhan 430062, P. R. China

*Corresponding author.

[*]E-mail: shisx@mail.hust.edu.cn (Songxin Shi) & dwzeng@mail.hust.edu.cn (Dawen Zeng)

Peer-reviewed version available at *Nanomaterials* **2019**, *9*, 1628; doi:10.3390/nano9111628

ABSTRACT: In this work, TiO_2 QDs modifed NiO nanosheets was employed to imporve the room-temperature NO_2 sensing properties of NiO. The gas-sensing studies showed that the response of nanocomposites with the optimal ratio to 60 ppm NO_2 was nearly 10 times larger than that of bare NiO, exhibiting potential application in gas-sensing. Considering the commonly reported immature mechanism that the effective charge transfer between two phases contribute to enhanced sensitivity, QDs sensitization mechanism was further detailed by designing a seirs of contrast experiments. First, the important role of QDs size effect was revealed by comparing a little enhanced sensitivity of TiO_2 particle-modified NiO with largely enhanced senstivity of TiO_2 QDs-NiO. Second, and more important, the direct evidence of heterointerface charge transfer efficiency was detailed by extracted interface bond (Ti-O-Ni) using XPS peak fitting. We hope this work can provide guideline to design more QDs-modified nanocomposites with the higher sensitivty for practical application.

Keywords: TiO_2 QDs; NiO nanosheets; NO_2; quantum size; heterointerface

Peer-reviewed version available at *Nanomaterials* **2019**, *9*, 1628; doi:10.3390/nano9111628

1. Introduction

Recently, quantum dots (QDs) have attracted great attention in various fields due to its large specific surface area, quantum size effects and single crystal structure with higher stability. [1-8] Especially, as a kind of surface modifier, semiconducting QDs was widely employed to improve the gas-sensing properties of metal-oxide-semiconductor (MOS) based materials, taking advantage of QDs size-induced active sites and the formation of heterojunction. [9-13] It was generally believed that the effective charge transfer between QDs and MOS contribute to the enhanced sensitivity of QDs-decorated sensing materials. For instance, $CuInS_2$ QDs modified NiO nanosheets exhibited enhanced sensitivity to NO_2 at room temperature compared to the bare NiO nanosheets. [14] The authors attributed this enhanced sensitivity to the effective heterointerface charge transfer between NiO nanosheets and $CuInS_2$ QDs. However, the effect of QDs size on the sensing properties of nanocomposites was not involved, because the charge transfer efficiency is largely dependent on QDs size due to the changes of energy band structure and specific surface area in QDs with different sizes. Moreover, the widely reported reason for the enhanced sensitivity is always based on the qualitative description of heterointerface charge transfer, lacking the corresponding evidence. In that case, the imperfection of QDs sensitization mechanism will certainly lead to obstacle for the further improvement of sensing properties.

NO_2, as a major air pollutant, has caused many problems, such as acid rain, photo-chemical smog, respiratory diseases, etc.[15-17] Meanwhile, the human chronic obstructive pulmonary disease can be monitored by measuring the concentration of NO_x in exhaled gases.[17-20]

Peer-reviewed version available at *Nanomaterials* **2019**, *9*, 1628; doi:10.3390/nano9111628

Therefore, it is urgent to design NO_2 sensors with higher sensing performance. NiO, a p-type metal-oxide semiconductor, is considered as a promising room-temperature NO_2 sensing material because of its high adsorption energy and great changes in electronic structure under the adsorption of NO_2 gas. [21-23] However, in actual NO_2 detection, bare NiO usually fails to meet the higher requirements in limit detection concentration.[24, 25] Therefore, it is vital to improve the sensing properties of bare NiO by modification. TiO_2 is an eco-friendly n-type metal oxide semiconductor with strong chemical and thermal stability.[26, 27] Meanwhile, TiO_2 can detect NO_2 gas at elevated temperature.[28, 29] Basing on the highly surface activity and appropriate energy band structures of TiO_2 QDs, it is reasonable to believe that TiO_2 QDs modification can improve the room temperature NO_2 sensing performance of bare NiO.

In this work, NiO nanosheets modified with different amount of TiO_2 QDs were firstly prepared. It was found that the room temperature NO_2 sensing performances of nanohybrids were significantly enhanced compared to the bare NiO nanosheets, indicating the important role of TiO_2 QDs. What's more, to further clarify the quantum size effects, NiO nanosheets modified with different sizes of TiO_2 nanoparticles were subsequently prepared. The results show that the sensitivity of the nanohybrids increased with both the increase in quantity of TiO_2 nanoparticles of the same particle size and the decrease of TiO_2 nanoparticle size. It was believed that the TiO_2 QDs with appropriate energy band structure could form effective heterojunction with NiO nanosheet, facilitating the effective charge transfer. To confirm this, on the basis of different nanocomposites with different amounts of TiO_2 QDs or TiO_2 nanoparticle, interface bonds (Ni-O-Ti) were extracted by XPS fitting. It was found that the variation of interface bond are in

Peer-reviewed version available at *Nanomaterials* **2019**, *9*, 1628; doi:10.3390/nano9111628

accordance with the sensitivity, directly indicating the enhanced heterointerface charge transfer efficiency in TiO_2 QDs-modified NiO nanosheets with optimal ratio due to the larger number of interface bonds. We hope this work could help us to deepen the understanding of the sensing mechanism of QDs-based nanohybrids and to design more QDs modified nanohybrids with the higher sensing performances.

Peer-reviewed version available at *Nanomaterials* **2019**, *9*, 1628; doi:10.3390/nano9111628

2. Experimental

2.1. Synthesis of TiO_2 QDs. On the basis of the process reported by Zaharescu,[30] we successfully synthesized TiO_2 QDs. Firstly, slowly pour in n-butanol (AR; 99.5%; 150 mL) to a three-necked flask (250 mL). Secondly, on a magnetic stirrer, concentrated nitric acid (65.0%～68.0%, 0.55 mL) and 0.81 mL of deionized water were slowly drop into the three-necked flask orderly at room temperature. Thirdly, nitrogen was introduced in the three-necked flask, and titanium butoxide (AR; 98.0%; 6.8 mL) was dropwise added to the solution with stirring for 30 minutes. Finally, transfer the solution to a reactor at 200 ° for 8 hours then naturally cooled to room temperature, and the nominal concentration of the prepared TiO_2 QDs solution is 0.21 mg/mL.

2.2. Synthesis of the NiO nanosheets. As shown in Fig. S1, 6 g of nickel chloride (AR; ⩾ 98.0%) was first dissolved in 300 mL of distilled water. Secondly, adjusted the solution pH to 10.0 by adding ammonia solution (AR; 28%). Thirdly, transfered the solution to a reactor at 160 ° for 6 hours then naturally cooled to room temperature. Finally, washed the precipitate three times with distilled water and ethanol by centrifugation at 8000 rpm, and the sample obtained after drying at 80 ºC.

2.3. Synthesis of TiO_2 QDs and TiO_2 nanoparticles decorated NiO nanosheets. Firstly, 0.001 mol NiO nanosheets dispersed in 50 mL n-hexane. Secondly, different volumes of TiO_2 QDs solution (1 ml, 2 mL, 5 mL and 10 mL) added respectively in the prepared NiO nanosheets solution, and treated by ultrasonic wave for 30 minutes to ensure the adequate mixing. Finally, washed the precipitate three times with water and distilled by centrifugation at 3000 rpm, and the samples obtained after drying at 80 ºC. The NiO nanosheets nanosheets added with different volumes of

Peer-reviewed version available at *Nanomaterials* **2019**, *9*, 1628; doi:10.3390/nano9111628

TiO_2 QDs solution named 1TiO_2QDs-NiO, 2TiO_2QDs-NiO, 5TiO_2QDs-NiO and 10TiO_2QDs-NiO, respectively. For comparison, the bare NiO nanosheets and the bare TiO_2 QDs were also prepared for testing.

Firstly, different quantity of TiO_2 nanoparticles (0.001 g, 0.002 g, 0.005 g, 0.010 g, 0.050 g, 0.100 g, 0.200 g) with diameters of 15nm and 30nm respectively (AR; ⩾99.9%, Shanghai XinZuan Alloy Material Co.) were added to 0.01 mol bare NiO nanosheets for full grinding. Secondly, the sintering processes was performed in an electric oven, which was maintained at a temperature of 200 ºC for 30 min and then naturally cooled to room temperature. Finally, the NiO nanosheets modified with different quantity of TiO_2 nanoparticles obtained, and denoted as 1$TiO_2$15-NiO, 2$TiO_2$15-NiO, 5$TiO_2$15-NiO, 10$TiO_2$15-NiO, 20$TiO_2$15-NiO, 50$TiO_2$15-NiO, 100$TiO_2$15-NiO, 1$TiO_2$30-NiO, 2$TiO_2$30-NiO, 5$TiO_2$30-NiO, 10$TiO_2$30-NiO, 20$TiO_2$30-NiO, 50$TiO_2$30-NiO and 100$TiO_2$30-NiO, respectively.

2.4. Characterization. Transmission electron microscopy (TEM, Tecnai G2F20 U-TWIN, 200kV, Japan) was carried out to observe the morphologies of the samples. The phase structure and chemical compositions were analyzed by X-ray photoelectron spectroscopy (XRD, X'pert PRO, PANalytical B.V., Almelo, the Netherlands, CuKα radiation with λ=0.15406 nm) from 10º to 90º. The valence band spectra and the surface compositions and tested by X-ray photoelectron spectroscopy (XPS, VG Multilab 2000X, Thermo Fisher Scientific Inc., Waltham, MA), and the binding energies were referenced to the C 1s peak at 284.6 eV. Tested in ultrahigh vacuum (UHV) container, He I excitation (21.2 eV) was used to detect the ultraviolet photoelectron spectroscopy (UPS) spectrum.

Peer-reviewed version available at *Nanomaterials* **2019**, *9*, 1628; doi:10.3390/nano9111628

2.5. Fabrication of gas sensors. Based on previous research in our laboratory[31, 32], the suspension was prepared to a solid membrane by thick film technology and its gas sensitivity was tested. Firstly, gold interdigital electrode printed on alumina ceramic sheet by screen printing process (Fig. S2). Secondly, suspension was prepared by mixing 20 mg of prapared powder with 0.2 mL ethanol. Thirdly, two microliters of prepared suspension were dropped on the gold interdigital electrode. Finally, the fabricated sensors were naturally air-dried and then in a thermostat at 80 ºC for 24 h.

2.6. Gas sensing performance testing. In our previous work, we described the test platform in detail,[33] which is equipped with data acquisition system and gas distribution device. Before the test, the gas sensors were installed in the test chamber, and then rinse with dry air for 30 minutes. Afterwards, different concentrations of NO_2 are obtained by mixing high concentration NO_2 with dry air, and the general flow was controlled at 1 L/min. The detailed testing process is as follows: 1) Injected in dry air for 100 s. 2) Injected in testing gas for 400 s. 3) Injected in dry air for 500 s. At room temperature, complete desorption of NO_2 molecules from nickel matrix composites is impossible. In order to ensure the repeatability and reliability of the test, before each test samples were heated at 80 ºC for 24 hours to eliminate residual NO_2 molecules and restore to original state.

In this study, the gas sensing performance is evaluated by response value (S), and the response value was evaluated by following formula:

$$S=\frac{R_o\text{-}R_g}{R_o} \qquad (1)$$

Where R_o and R_g represent the resistance values of the sensors in air and the target gas

Peer-reviewed version available at *Nanomaterials* **2019**, *9*, 1628; doi:10.3390/nano9111628

respectively.

3. Results and discussions

3.1. Gas sensing performances. For the TiO_2 QDs modified NiO nanosheets, the dynamic sensitivity-recovery curves and responses versus NO_2 concentration (5-60 ppm) at room temperature are show in Fig. 1a-b. The results show that, compared with the bare NiO nanosheets, the sensitivity to NO_2 of TiO_2QDs-NiO nanohybrids are significantly improved. More importantly, the sensitivity values are increased with increase the quantity of TiO_2 QDs, and decreased slightly when the QDs solution is added in excess of 5 ml. Responses of the nanohybrids modified by different sizes of TiO_2 nanoparticles to 60 ppm NO_2 at room temperature are shown in Fig. 1c. The result show that the responses of the nanohybrids increase with the diminution of TiO_2 nanoparticle size. At the same time, with the increase of TiO_2 content of the same nanoparticle size, the response value first increases and then decreases too. Samples 5TiO_2QDs-NiO, 20$TiO_2$15-NiO, and 50$TiO_2$30-NiO obtain the maximum response in their respective sample populations, and the response values are 18.5, 4.4, and 2.7, respectively.

Peer-reviewed version available at *Nanomaterials* **2019**, *9*, 1628; doi:10.3390/nano9111628

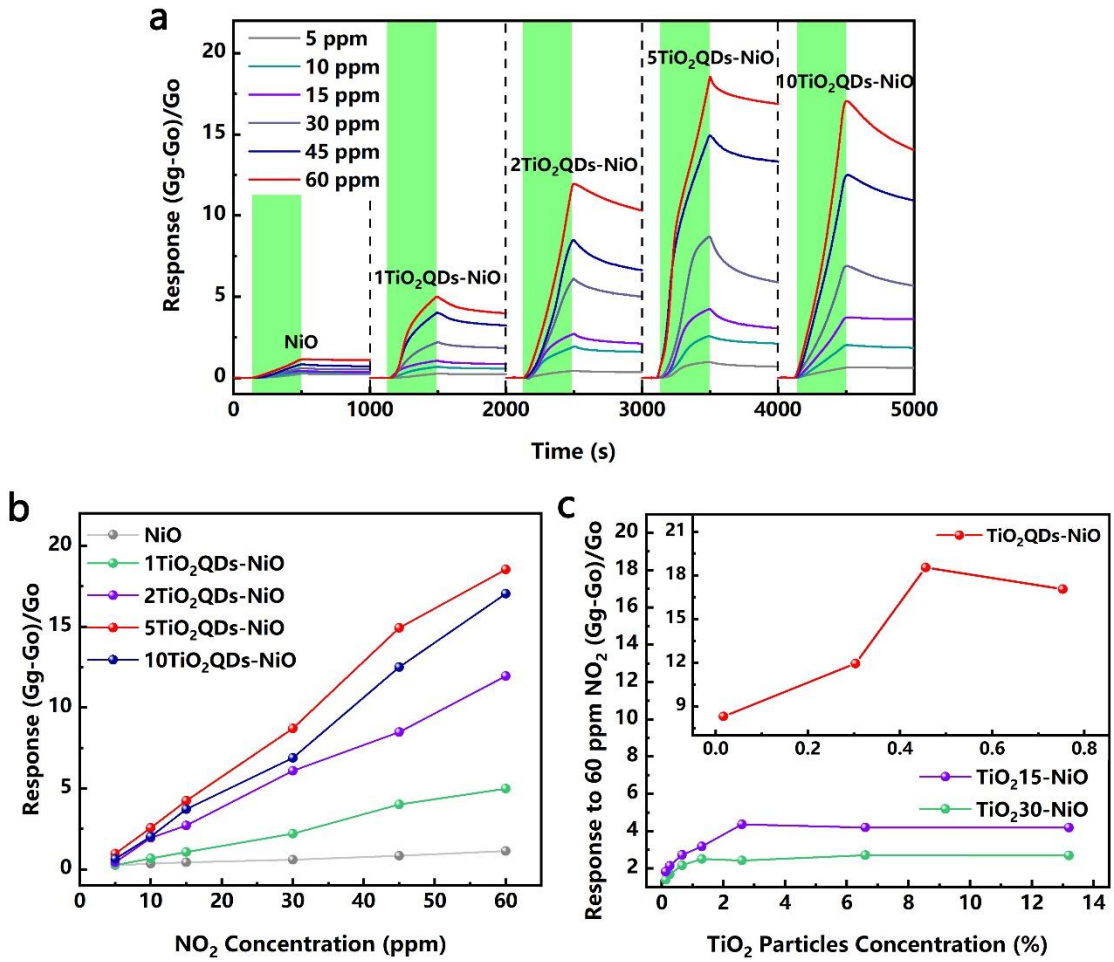

Fig. 1. (a) Dynamic sensitivity-recovery curves and (b) responses of the bare NiO nanosheets and the NiO nanosheets modified with different quantity of TiO_2 QDs to different concentration of NO_2 at room temperature; (c) Responses of NiO nanosheets modified with different sizes of TiO_2 nanoparticle to 60 ppm NO_2 at room temperature.

As shown in Fig. S3a, to observe the selectivity of the prepared TiO_2QDs-NiO nanohybrids, different kinds of gases, including NO_2, n-butyl alcohol, CO, benzene, NH_3, H_2, and isoprene are detected. Among these gases, sample 5TiO_2QDs-NiO exhibits the highest response to NO_2, which proves that the prepared nanohybrids have excellent electivity. Furthermore, the gas sensitivity of the 5TiO_2QDs-NiO at 60 PPm to NO_2 is taken to test the repeatability of the material's gas sensitive performance, and the dynamic sensitivity-recovery curves are shown in Fig. S3b. The results show that the prepared nanohybrids have excellent repeatability.

Peer-reviewed version available at *Nanomaterials* **2019**, *9*, 1628; doi:10.3390/nano9111628

3.2. Structure characterization. Are shown in Fig. S4a, the XRD patterns of the NiO nanosheets and the TiO_2 QDs modified NiO nanosheets are indexed to the cubic NiO (JCPDS, ICDD no. 78-0423). There are no characteristic peaks for impurity are observed, which indicates that the prepared samples have high purity. At the same time, the diffraction peaks of TiO_2 are not shown in the patterns for the reason of the low quantity of TiO_2. Furthermore, to illustrate the QDs concentration of the TiO_2QDs-NiO nanohybrids, the XPS spectra also employed. As shown in Fig. S4b, with increase the quantity of TiO_2 QDs, concentration of Ti 2p of the samples also increase. The XRD patterns of the 20$TiO_2$15-NiO and the 50$TiO_2$30-NiO obtain the maximum response in their respective sample populations are shown in Fig. S4c-d. Except the XRD peaks of cubic NiO (JCPDF No. 08-0237) labeled by hollow circle, all the other diffraction peaks marked by solid circle are designated to the anatase TiO_2 (JCPDS No. 21–1272), suggesting that the nanohybrids have been successfully prepared and do not contain impurities obviously.

In order to observe the microstructure information of the prepared samples, TEM was utilized. As shown in Fig. 2, the TEM images that the bare NiO are composed of nanosheets containing micropores, the synthetic TiO_2 QDs are nanoscale black dots, the TiO_2 QDs and TiO_2 nanoparticles are uniformly separated on the surface of the NiO nanosheets. Meanwhile, the lattice spacings are measured to be 0.35 nm in the high magnification TEM images (Fig. 2d-f) is attached to the (101) planes of anatase TiO_2. By measurement, the diameter of TiO_2 QDs and TiO_2 nanoparticles were 3nm, 15nm and 30nm, respectively.

Peer-reviewed version available at *Nanomaterials* **2019**, *9*, 1628; doi:10.3390/nano9111628

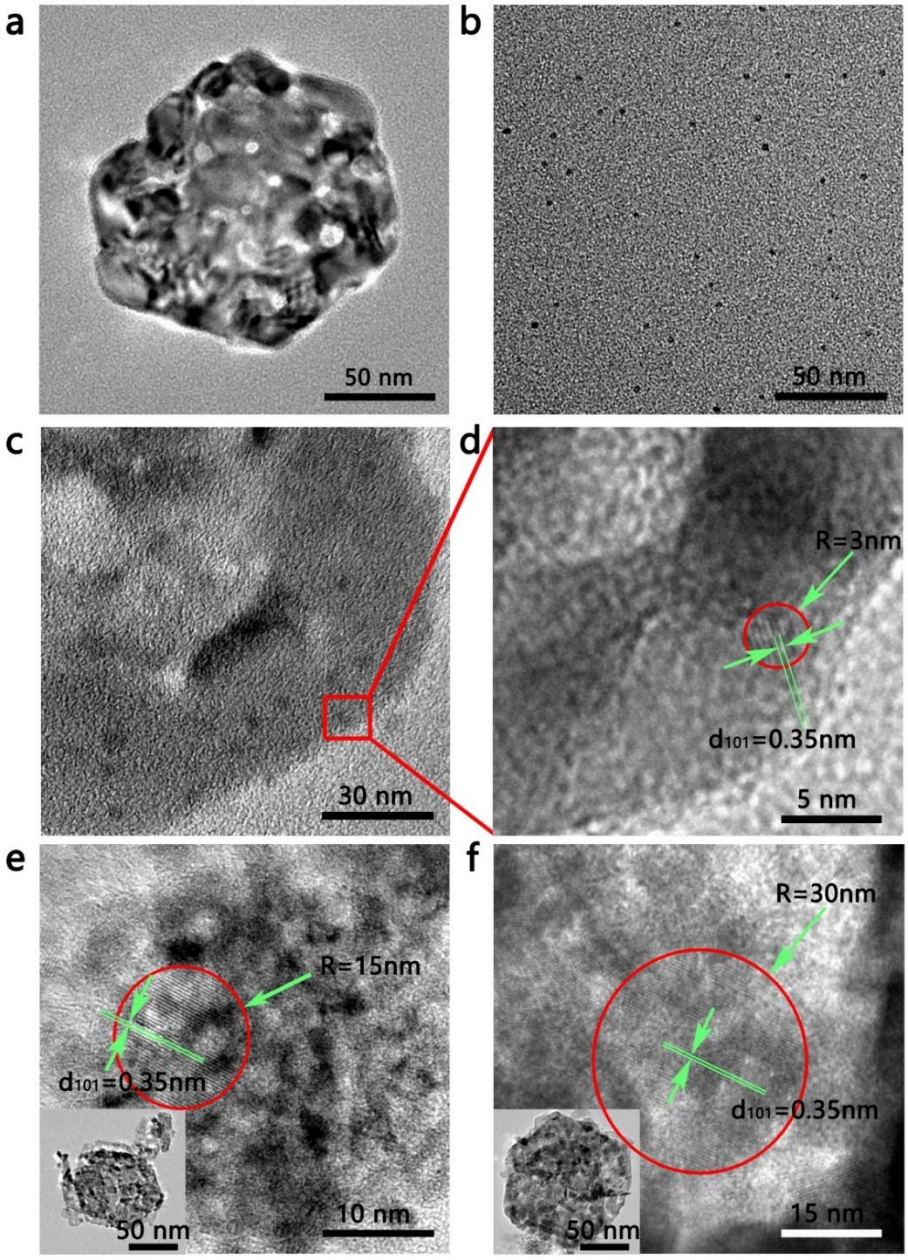

Fig. 2. The TEM images of (a) the bare NiO nanosheets, and (b) the bare TiO_2 QDs. The low- and the high-magnification of (c, d) the TiO_2QDs-NiO, (e) the $TiO_2$15-NiO and (f) the $TiO_2$30-NiO.

3.3. Energy band structure of the TiO_2 QDs. It is well known that the preparation process of QDs will affect the properties of QDs. In order to elaborate the influence of TiO_2 QDs on the gas sensing properties of NiO nanosheets, it is necessary to determine the energy band structure of the TiO_2 QDs. As shown in Fig. 3, UPS, valence band XPS spectrum and UV-vis spectroscopy are

Peer-reviewed version available at Nanomaterials 2019, 9, 1628; doi:10.3390/nano9111628

performed to calculate the energy band structure of TiO_2 QDs. As shown in Fig. 3a, the E_{vac} is 21.2 eV above the spectrum of cutoff energy,[34] and the work function of the prepared TiO_2 QDs is 3.375 eV. Meanwhile, the valence band of the TiO_2 QDs is shown in Fig. 3b, the position of the top of valence band is up to the crossing point of the linear fitting for the light emission front of the valence band,[35] and the maximum position of TiO_2 QDs is 1.8 eV lower than the Fermi energy level. The ultraviolet visible (UV-vis) absorption spectrum of TiO_2 QDs is shown in Fig. 3c, and the band gap of the TiO_2 QDs is 3.7 eV. Through the above analysis, the energy band structure of TiO_2 QDs is shown in Fig. 3d.

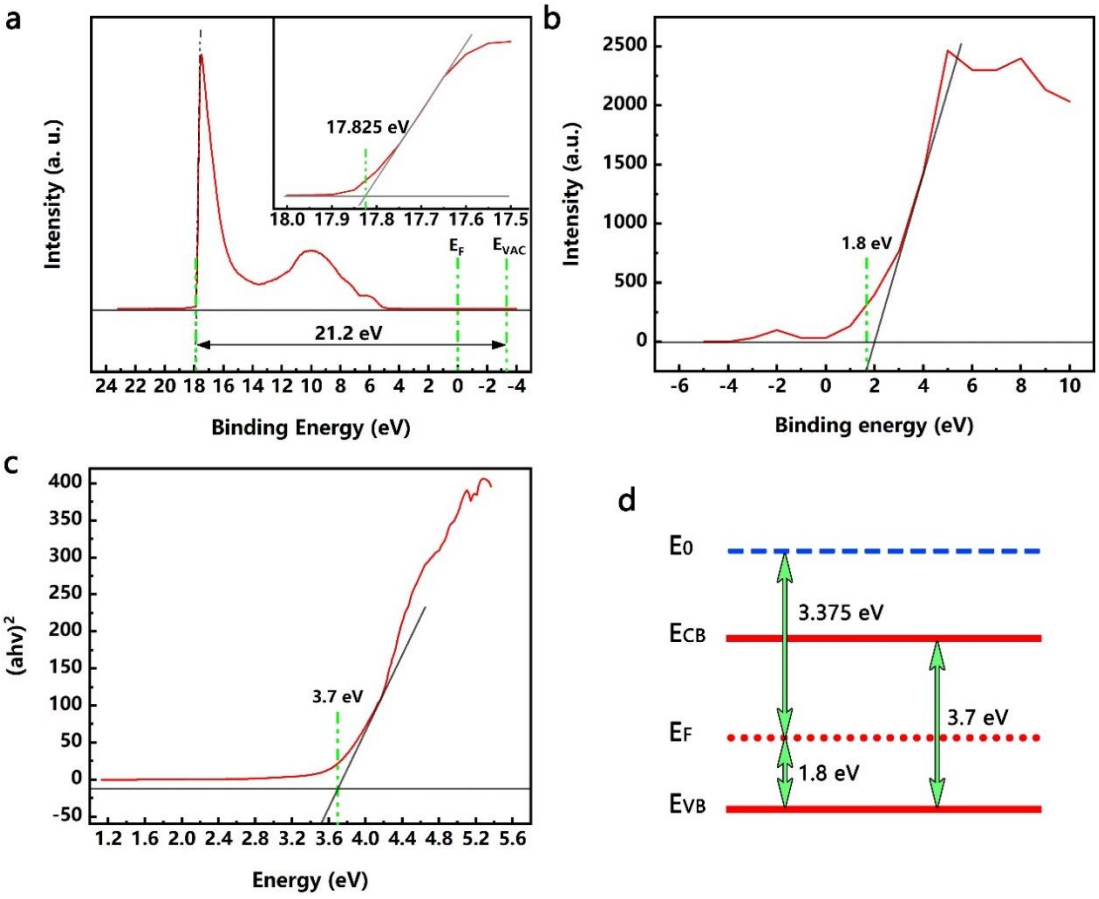

Fig. 3. (a) The UPS spectra of TiO_2 QDs; (b) The XPS spectrum of TiO_2 QDs; (c) The plot of $(\alpha h\upsilon)^2$ against photon energy ($h\upsilon$) for TiO_2 QDs; (d) The corresponding energy band structure o TiO_2 QDs based on the UPS, XPS and UV-vis results.

Peer-reviewed version available at *Nanomaterials* **2019**, *9*, 1628; doi:10.3390/nano9111628

3.4. Sensing mechanism. NiO is a p-type metal-oxide semiconductor and hole (h^+) is the main carrier, which produced by the ionization of neutral Ni vacancy ($V_{Ni}^{\times}$), (Equation (2)).[33, 36] During the gas sensitivity measurement, NO_2 gas molecules first adsorb on the surface of NiO, as expressed by (Eq. (3)). After that, the NO_2 gas molecules obtain electrons from doubly charged nickel vacancy ($V_{Ni}^{''}$) and form singly charged nickel vacancy ($V_{Ni}^{'}$) (Eq. (4)). Meanwhile, the consumption of $V_{Ni}^{''}$ can promote the ionization of $V_{Ni}^{\times}$ and generate more holes that help to increase the conductivity of the nanohybrid. The reactions on the surface of the nanohybrid can be expressed as follows:

$$V_{Ni}^{\times} \leftrightarrow V_{Ni}^{''} + 2h^{+} \quad (2)$$

$$NO_2(gas) \rightarrow NO_2(ads) \quad (3)$$

$$NO_2(ads) + V_{Ni}^{''} \rightarrow NO_2^{-} - V_{Ni}^{'} \quad (4)$$

As for the TiO_2 QDs decorated NiO nanosheets, comparing to the bare NiO nanosheets, the response versus NO_2 at room temperature is significantly improved, while the response of TiO_2 QDs versus NO_2 is very weak (Fig. S8), indicating that the improvement of gas-sensitive performance was caused by the interaction of materials. Furthermore, in order to detail the effect of QDs on the gas sensing performances, large TiO_2 nanoparticles (15 nm, 30 nm) modified NiO nanosheets were also prepared. As shown in Figure 1c, with increasing the quantity of TiO_2 of the same nanoparticle size, the response value first increases and then slightly decreases. Meanwhile, the response of the nanohybrids increase with the diminution of TiO_2 nanoparticle size. Based on the energy band structure of the n-type TiO_2 QDs, it was reasonable to believe that the variation of heterointerfaces help to the enhancement of sensitivity. As shown in Fig. 4, the XPS spectra of the

Peer-reviewed version available at *Nanomaterials* **2019**, *9*, 1628; doi:10.3390/nano9111628

nanohybrids can be deconvoluted to six peaks, coinciding with the peaks of Ni $2p_{1/2}$ and Ni $2p_{3/2}$. Of particular note, compared with NiO nanosheets, the binding energies for the Ni 2p of the TiO_2 modified nanohybrids shift to higher values.[37, 38] More importantly, as shown in Fig. 4a-b, for the TiO_2QDs-NiO nanohybrids, the shift value first increases and then decreases with the increase of TiO_2 QDs content, which is consistent with the change of response value too. Meanwhile, as shown in Fig. 4c-d, for the samples 5TiO_2QDs-NiO, 20$TiO_2$15-NiO and 50$TiO_2$30-NiO with the optimal performance in their respective sample populations, the shift value increases with the diminution of TiO_2 nanoparticle size, which is consistent with the change of response value too. The shift of binding energy is mainly due to the difference in the electronegativity of ions and the interfacial electron transfer between the NiO nanosheets and the TiO_2 nanoparticles.[39] Comparing the energy band structure of the NiO nanosheets and the TiO_2 QDs,[40-42] as shown in Fig. 5a, in order to achieve the equalization of the Fermi levels, electrons are transferred from TiO_2 QDs to NiO nanosheets.

Peer-reviewed version available at *Nanomaterials* **2019**, *9*, 1628; doi:10.3390/nano9111628

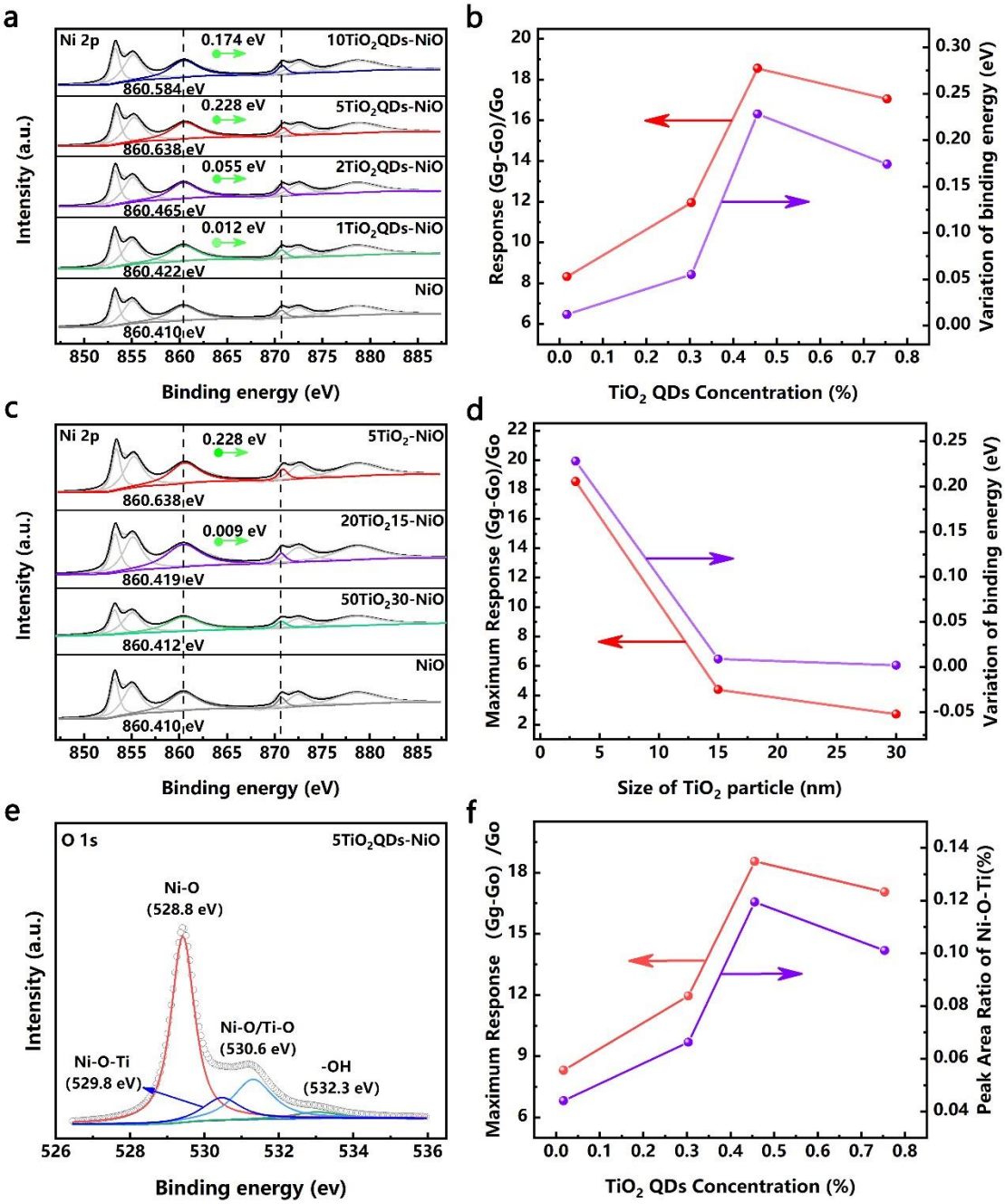

Fig. 4. (a) Ni 2p spectra of the bare NiO and the TiO_2QDs-NiO nanohybrids. (b) With the increase of TiO_2 QDs content, comparison between the variation of the responses to 60 ppm NO_2 and the variation of the binding energy shift values. (c) Ni 2p spectra of the bare NiO and the 5TiO_2QDs-NiO, 20TiO215-NiO and 50TiO230-NiO. (d) With the increase of TiO_2 nanoparticle size, comparison between the variation of the maximum responses to 60 ppm NO_2 and the variation of the binding energy shift values. (e) O 1s spectra of the 5TiO_2QDs-NiO. (f) With the increase of TiO_2 QDs content, comparison between the variation of the responses to 60 ppm NO_2 and the variation of the peak area ratio of Ni-O-Ti.

Furthermore, the change of heterointerface can be judged by the change of interfacial bond

Peer-reviewed version available at Nanomaterials 2019, 9, 1628; doi:10.3390/nano9111628

content. As shown in Fig. 4e, the O1s high resolution XPS spectra of the sample can be deconvoluted into four peaks with binding energies of 528.8, 529.8, 530.6, 532.3 eV. [43-46] The peak at 528.8 eV can be ascribed to the lattice oxygen in NiO; The peak at 529.8 eV is identified to the Ni-O-Ti bond; The peak at 530.6 eV can be ascribed to the defective oxygen in NiO and the crystal lattice oxygen in TiO_2;[47, 48] The peak at 532.2 eV can be ascribed to the hydroxyl oxygen and water molecules on the surface of the mesoporous NiO; As shown in Fig. 4f and Fig. S5, for the TiO_2QDs-NiO nanohybrids, the peak area ratio of Ni-O-Ti bond first increases and then decreases with the increase of TiO_2 QDs content, which is consistent with the change of response value. Meanwhile, as shown in Fig. S6-7, for the samples 5TiO_2QDs-NiO, 20$TiO_2$15-NiO and 50$TiO_2$30-NiO with the optimal performance in their respective sample populations, the peak area ratio of Ni-O-Ti bond increases with the diminution of TiO_2 nanoparticle size, which is consistent with the change of response value too. These results clearly show that TiO_2 QDs could offer a larger number of heterointerfaces than large TiO_2 nanoparticles of equivalent mass, while the increase in quantity of TiO_2 nanoparticles of the same particle size would also increase the content of heterointerfaces, which help to improve the charge transport efficiency.

As shown in Fig. 5b, when the NiO nanosheets is contacted with the TiO_2 QDs， compared to large TiO_2 nanoparticles, larger number of heterointerfaces are formed which can greatly improve the transfer efficiency of electronic. Upon exposure to NO_2, the ultra-efficient electron transfer based on more heterointerfaces from TiO_2 QDs to NiO nanosheets could extremely promote the ionization reaction of the neutral Ni vacancy, and more quantities of charged Ni vacancies would participate in the NO_2 sensing reaction(Eq.(4)). Hence, as shown in Fig. 5c, for the surface band

Peer-reviewed version available at *Nanomaterials* **2019**, *9*, 1628; doi:10.3390/nano9111628

bending, TiO_2 QDs modified NiO nanosheets, large TiO_2 nanoparticles modified NiO nanosheet and the bare NiO nanosheets are in descending order, which is consistent with the change in gas sensitivity.

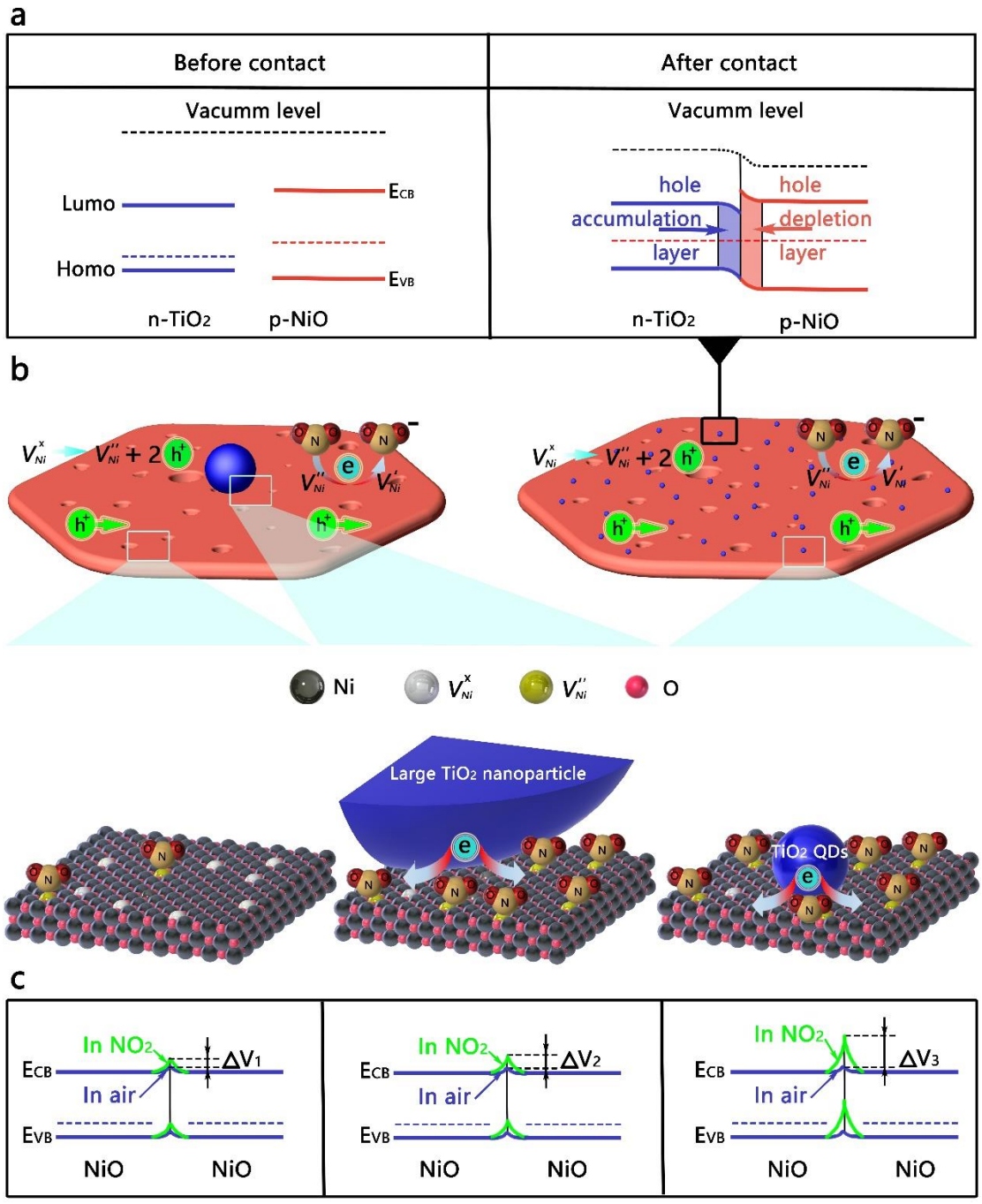

Fig. 5. (a) The energy band diagram of as-prepared samples, before and after contact. (b) The schematic of the interfacial interaction between the TiO_2-NiO_2 nanohybrids structure and NO_2 molecules. (c) Comparison of the

Peer-reviewed version available at *Nanomaterials* **2019**, *9*, 1628; doi:10.3390/nano9111628

surface band bending between NiO nanosheets, large TiO_2 nanoparticle modified NiO nanosheets and TiO_2 QDs modified NiO nanosheets.

Furthermore, the quantity of holes in NiO nanosheets reduced with the electrons transferred from the TiO_2 QDs to the NiO nanosheets, which results in the reduction of initial conductivity of the nanohybrids (Fig. S9). According to the definition of sensitivity, the reduction of initial conductivity in the air conduce to improve the sensitivity of the nanohybrid. For the NiO nanosheets modified with different quantities of TiO_2 nanoparticles of the same particle size, the room temperature sensitivity increased with the increase of TiO_2 nanoparticles. When the quantity of TiO_2 nanoparticles further increased, the sensitivity of the nanohybrids decreased slightly. The possible reason is that the heterointerfaces are increased with the increase of TiO_2 nanoparticles, but further increasing the quantity of TiO_2 nanoparticles could occupy the reactive site for gas sensing and there will be agglomeration, leading to slightly decreased of the sensitivity.[14]

Peer-reviewed version available at *Nanomaterials* **2019**, *9*, 1628; doi:10.3390/nano9111628

4. Conclusions

In summary, by comparing the sensitivity of NiO nanosheets modified by different content of TiO_2 QDs and different size of TiO_2 nanoparticles, the effect of QDs on the gas sensing performances of nanohybrid is discussed in detail from the two dimensions of concentration and nanoparticle size, taking the heterointerface as the core. For the NiO nanosheets modified by different content of TiO_2 QDs, the binding energy shift value and the peak area ratio of Ni-O-Ti bond first increases and then decreases with the increase of TiO_2 QDs content, which is consistent with the change of respond value. Meanwhile, for the samples with the optimal performance in their respective sample populations binding energy shift value and the peak area ratio of Ni-O-Ti bond increased with the diminution of TiO_2 nanoparticle size, which is consistent with the change of response value too. It was believed that the increase in quantity of TiO_2 QDs will increase the content of heterointerfaces, while TiO_2 QDs could offer more heterointerfaces than large TiO_2 nanoparticles. Moreover，according to the definition of the response value, reducing the initial conductance helps to improve the sensitivity of the materials. Through this work, we can better understand the impact of quantum size on the QDs sensitization mechanism on the variation of heterointerfaces.

Peer-reviewed version available at *Nanomaterials* **2019**, *9*, 1628; doi:10.3390/nano9111628

AUTHOR INFORMATION

Corresponding Author

*E-mail: shisx@mail.hust.edu.cn (Songxin Shi) & dwzeng@mail.hust.edu.cn (Dawen Zeng)

Author Contributions

The manuscript was written through contributions of all authors. All authors have given approval to the final version of the manuscript.

Notes

There are no conflicts to declare.

ACKNOWLEDGEMENTS

The authors gratefully acknowledge the financial support by the Aeronautical Science Foundation of China (Grant Nos. 20130379003), and the National Natural Science Foundation of China (Grant Nos. 51572075). Moreover, we thank the technology support by the Analytic Testing Center of HUST for carrying out XRD, FESEM, HRTEM, and XPS.

Peer-reviewed version available at *Nanomaterials* **2019**, *9*, 1628; doi:10.3390/nano9111628

REFERENCES

1. F. Y. Shen, W. X. Que, Y. C. He, Y. Yuan, X. T. Yin and G. F. Wang, "Enhanced Photocatalytic Activity of ZnO Microspheres via Hybridization with CuInSe2 and CuInS2 Nanocrystals," *Acs Applied Materials & Interfaces*, vol. 4, no. 8, pp. 4087-4092, 2012.

2. M. Y. Cha, P. M. Da, J. Wang, W. Y. Wang, Z. H. Chen, F. X. Xiu, G. F. Zheng and Z. S. Wang, "Enhancing Perovskite Solar Cell Performance by Interface Engineering Using CH3NH3PbBr0.9I2.1 Quantum Dots," *Journal of the American Chemical Society*, vol. 138, no. 27, pp. 8581-8587, 2016.

3. L. Y. Zhu, W. J. An, J. W. Springer, L. B. Modesto-Lopez, S. Gullapalli, D. Holten, M. S. Wong and P. Biswas, "Linker-free quantum dot sensitized TiO2 photoelectrochemical cells," *International Journal of Hydrogen Energy*, vol. 37, no. 8, pp. 6422-6430, 2012.

4. L. Pan, J. J. Zou, S. B. Wang, Z. F. Huang, A. Yu, L. Wang and X. W. Zhang, "Quantum dot self-decorated TiO2 nanosheets," *Chemical Communications*, vol. 49, no. 59, pp. 6593-6595, 2013.

5. R. Danish, F. Ahmed and B. H. Koo, "Rapid synthesis of high surface area anatase Titanium Oxide quantum dots," *Ceramics International*, vol. 40, no. 8, pp. 12675-12680, 2014.

6. M. F. Frasco and N. Chaniotakis, "Semiconductor Quantum Dots in Chemical Sensors and Biosensors," *Sensors*, vol. 9, no. 9, pp. 7266-7286, 2009.

7. Y. L. Liu, L. L. Wang, H. R. Wang, M. Y. Xiong, T. Q. Yang and G. S. Zakharova, "Highly sensitive and selective ammonia gas sensors based on PbS quantum dots/TiO2 nanotube arrays at room temperature," *Sensors and Actuators B-Chemical*, vol. 236, pp. 529-536, 2016.

8. Z. L. Song, Z. R. Wei, B. Wang, Z. Luo, S. M. Xu, W. K. Zhang, H. X. Yu, M. Li, Z. Huang, J. F. Zang, F. Yi and H. Liu, "Sensitive Room-Temperature H2S Gas Sensors Employing SnO2 Quantum Wire/Reduced Graphene Oxide Nanocomposites," *Chemistry of Materials*, vol. 28, no. 4, pp. 1205-1212, 2016.

9. Z. Wei, H. Xi-Wen, C. Yang, L. Wen-You and Z. Yu-Kui, "Composite of CdTe quantum dots and molecularly imprinted polymer as a sensing material for cytochrome c," *Biosensors & Bioelectronics*, vol. 26, no. 5, pp. 2553-2558, 2011.

10. W. Peng, Z. Jinyi, W. Shanlin, Z. Airu and H. Xiandeng, "Sensing during in situ growth of Mn-doped ZnS QDs: a phosphorescent sensor for detection of H2S in biological samples," *Chemistry - A European Journal*, vol. 20, no. 4, pp. 952-956, 2014.

11. Y. S. Xia and C. Q. Zhu, "Use of surface-modified CdTe quantum dots as fluorescent probes in sensing mercury (II)," *Talanta*, vol. 75, no. 1, pp. 215-221, 2008.

12. M. Chao, X. Yao, W. Pan, Z. Lei, L. Yanxin and T. Limin, "Quantum-dot-doped polymer nanofibers for optical sensing," *Advanced Materials*, vol. 23, no. 33, pp. 3770-3774, 2011.

13. S. A. Waghuley, "LPG Sensing Application Of Graphene/CeO2 Quantum Dots Composite," in *Aip Proceeding*, Ed., 2013.

14. J. Zhang, D. Hu, S. Tian, Z. Qin, D. Zeng and C. Xie, "CuInS 2 QDs decorated ring-like NiO for significantly enhanced room-temperature NO 2 sensing performances via effective interfacial charge transfer," *Sensors & Actuators B Chemical*, vol. 256, 2017.

15. K. Li, L. Chen, K. Han, B. Lv, K. Bao, X. Wu, X. Gao and K. Cen, "Smog chamber study on aging of combustion soot in isoprene/SO2/NOx system: Changes of mass, size, effective density, morphology and mixing state," *Atmospheric Research*, vol. 184, pp. 139-148, 2017.

16. G. E. Likens and T. J. Butler, *Acid Rain: Causes, Consequences, and Recovery in Terrestrial, Aquatic, and Human*

Peer-reviewed version available at *Nanomaterials* **2019**, *9*, 1628; doi:10.3390/nano9111628

Systems, 2017.

17. M. Zhang, H. C. Su, Y. Rheem, C. M. Hangarter and N. V. Myung, "A Rapid Room-Temperature NO2 Sensor Based on Tellurium-SWNT Hybrid Nanostructures," *Journal of Physical Chemistry C*, vol. 116, no. 37, pp. 20067-20074, 2012.

18. K. Alving, E. Weitzberg and J. M. Lundberg, "Increased amount of nitric oxide in exhaled air of asthmatics," *The European respiratory journal*, vol. 6, no. 9, pp. 1368-1370, 1993.

19. A. D. Smith, J. O. Cowan, K. P. Brassett, G. P. Herbison and D. R. Taylor, "Use of exhaled nitric oxide measurements to guide treatment in chronic asthma," *New England Journal of Medicine*, vol. 352, no. 21, pp. 2163-2173, 2005.

20. S. P. Mondal, P. K. Dutta, G. W. Hunter, B. J. Ward, D. Laskowski and R. A. Dweik, "Development of high sensitivity potentiometric NOx sensor and its application to breath analysis," *Sensors and Actuators B-Chemical*, vol. 158, no. 1, pp. 292-298, 2011.

21. B. Liu, H. Yang, H. Zhao, L. An, L. Zhang, R. Shi, L. Wang, L. Bao and Y. Chen, "Synthesis and enhanced gas-sensing properties of ultralong NiO nanowires assembled with NiO nanocrystals," *Sensors and Actuators B-Chemical*, vol. 156, no. 1, pp. 251-262, 2011.

22. H. J. Kim and J. H. Lee, "Highly sensitive and selective gas sensors using p-type oxide semiconductors: Overview," *Sensors and Actuators B-Chemical*, vol. 192, pp. 607-627, 2014.

23. B. C. Wang, J. Nisar and R. Ahuja, "Molecular Simulation for Gas Adsorption at NiO (100) Surface," *Acs Applied Materials & Interfaces*, vol. 4, no. 10, pp. 5691-5697, 2012.

24. J. Zhang, D. W. Zeng, Q. Zhu, J. J. Wu, K. Xu, T. G. Liao, G. Z. Zhang and C. S. Xie, "Effect of Grain-Boundaries in NiO Nanosheet Layers Room-Temperature Sensing Mechanism under NO2," *Journal of Physical Chemistry C*, vol. 119, no. 31, pp. 17930-17939, 2015.

25. J. Zhang, D. W. Zeng, Q. Zhu, J. J. Wu, Q. W. Huang and C. S. Xie, "Effect of Nickel Vacancies on the Room-Temperature NO2 Sensing Properties of Mesoporous NiO Nanosheets," *Journal of Physical Chemistry C*, vol. 120, no. 7, pp. 3936-3945, 2016.

26. M. M. Khan, S. A. Ansari, D. Pradhan, M. O. Ansari, D. H. Han, J. Lee and M. H. Cho, "Band gap engineered TiO2 nanoparticles for visible light induced photoelectrochemical and photocatalytic studies," *Journal of Materials Chemistry A*, vol. 2, no. 3, pp. 637-644, 2014.

27. S. Kalathil, M. M. Khan, S. A. Ansari, J. Lee and M. H. Cho, "Band gap narrowing of titanium dioxide (TiO2) nanocrystals by electrochemically active biofilms and their visible light activity," *Nanoscale*, vol. 5, no. 14, pp. 6323-6326, 2013.

28. A. M. Ruiz, G. Sakai, A. Cornet, K. Shimanoe, J. R. Morante and N. Yamazoe, "Cr-doped TiO 2 gas sensor for exhaust NO 2 monitoring," *Sensors & Actuators B Chemical*, vol. 93, no. 1, pp. 509-518, 2003.

29. Y. Yamada, Y. Seno, Y. Masuoka, T. Nakamura and K. Yamashita, "NO 2 sensing characteristics of Nb doped TiO 2 thin films and their electronic properties," *Sensors & Actuators B*, vol. 66, no. 1, pp. 164-166, 2000.

30. J. M. Calderon-Moreno, S. Preda, L. Predoana, M. Zaharescu, M. Anastasescu, M. Nicolescu, M. Stoica, H. Stroescu, M. Gartner, O. Buiu, M. Mihaila and B. Serban, "Effect of polyethylene glycol on porous transparent TiO2 films prepared by sol-gel method," *Ceramics International*, vol. 40, no. 1, pp. 2209-2220, 2014.

31. J. Zhang, D. W. Zeng, S. Q. Zhao, J. J. Wu, K. Xu, Q. Zhu, G. Z. Zhang and C. S. Xie, "Room temperature NO2 sensing: what advantage does the rGO-NiO nanocomposite have over pristine NiO?," *Physical Chemistry Chemical Physics*, vol. 17, no. 22, pp. 14903-14911, 2015.

Peer-reviewed version available at *Nanomaterials* **2019**, *9*, 1628; doi:10.3390/nano9111628

32. Z. B. Ye, H. L. Tai, T. Xie, Z. Yuan, C. H. Liu and Y. D. Jiang, "Room temperature formaldehyde sensor with enhanced performance based on reduced graphene oxide/titanium dioxide," *Sensors and Actuators B-Chemical*, vol. 223, pp. 149-156, 2016.

33. J. Zhang, J. J. Wu, X. X. Wang, D. W. Zeng and C. S. Xie, "Enhancing room-temperature NO2 sensing properties via forming heterojunction for NiO-rGO composited with SnO2 nanoplates," *Sensors and Actuators B-Chemical*, vol. 243, pp. 1010-1019, 2017.

34. W. J. Chun, A. Ishikawa, H. Fujisawa, T. Takata, J. N. Kondo, M. Hara, M. Kawai, Y. Matsumoto and K. Domen, "Conduction and valence band positions of Ta2O5, TaON, and Ta3N5 by UPS and electrochemical methods," *Journal of Physical Chemistry B*, vol. 107, no. 8, pp. 1798-1803, 2003.

35. H. P. Song, G. L. Zheng, A. L. Yang, Y. Guo, H. Y. Wei, C. M. Li, S. Y. Yang, X. L. Liu, Q. S. Zhu and Z. G. Wang, "The growth of ZnO on buffer layers and the valence band offset determined by X-ray photoemission spectroscopy," *Solid State Communications*, vol. 150, no. 41, pp. 1991-1994, 2010.

36. I. Castro-Hurtado, C. Malagu, S. Morandi, N. Perez, G. G. Mandayo and E. Castano, "Properties of NiO sputtered thin films and modeling of their sensing mechanism under formaldehyde atmospheres," *Acta Materialia*, vol. 61, no. 4, pp. 1146-1153, 2013.

37. G. Y. Hou, Y. Y. Xie, L. K. Wu, H. Z. Cao, Y. P. Tang and G. Q. Zheng, "Electrocatalytic performance of Ni-Ti-O nanotube arrays/NiTi alloy electrode annealed under H 2 atmosphere for electro-oxidation of methanol," *International Journal of Hydrogen Energy*, vol. 41, no. 22, pp. 9295-9302, 2016.

38. J. Liang, H. Tan, C. Xiao, G. Zhou, S. Guo and S. Ding, "Hydroxyl-riched halloysite clay nanotubes serving as substrate of NiO nanosheets for high-performance supercapacitor," *Journal of Power Sources*, vol. 285, no. ISSN, pp. 210-216, 2015.

39. L. Xu, R. F. Zheng, S. H. Liu, J. Song, J. S. Chen, B. Dong and H. W. Song, "NiO@ZnO Heterostructured Nanotubes: Coelectrospinning Fabrication, Characterization, and Highly Enhanced Gas Sensing Properties," *Inorganic Chemistry*, vol. 51, no. 14, pp. 7733-7740, 2012.

40. J. Bandara, C. M. Divarathne and S. D. Nanayakkara, "Fabrication of n-p junction electrodes made of n-type SnO2 and p-type NiO for control of charge recombination in dye-sensitized solar cells (vol 81, pg 2004, 429)," *Solar Energy Materials and Solar Cells*, vol. 85, no. 1, pp. 141-142, 2005.

41. J. Bandara and J. P. Yasomanee, "p-type oxide semiconductors as hole collectors in dye-sensitized solid-state solar cells," *Semiconductor Science and Technology*, vol. 22, no. 2, pp. 20-24, 2007.

42. J. C. Bernede, S. Houari, D. Nguyen, P. Y. Jouan, A. Khelil, A. Mokrani, L. Cattin and P. Predeep, "XPS study of the band alignment at ITO/oxide (n-type MoO3 or p-type NiO) interface," *Physica Status Solidi a-Applications and Materials Science*, vol. 209, no. 7, pp. 1291-1297, 2012.

43. M. Bonomo, A. G. Marrani, V. Novelli, M. Awais, D. P. Dowling, J. G. Vos and D. Dini, "Surface properties of nanostructured NiO undergoing electrochemical oxidation in 3-methoxy-propionitrile," *Applied Surface Science*, vol. 403, pp. 441-447, 2017.

44. J. L. Rodriguez, M. A. Valenzuela, T. Poznyak, L. Lartundo and I. Chairez, "Reactivity of NiO for 2,4-D degradation with ozone: XPS studies," *Journal of Hazardous Materials*, vol. 262, pp. 472-481, 2013.

45. Z. W. Li, "Supersensitive and superselective formaldehyde gas sensor based on NiO nanowires," *Vacuum*, vol. 143, pp. 50-53, 2017.

46. X. T. Yin, J. Liu, J. Q. Ma, C. X. Zhang, P. Chen, M. D. Que, Y. W. Yang, W. X. Que, C. M. Niu and J. Y. Shao, "Solvothermal derived crystalline NiOx nanoparticles for high performance perovskite solar cells," *Journal of Power*

Peer-reviewed version available at *Nanomaterials* **2019**, *9*, 1628; doi:10.3390/nano9111628

Sources, vol. 329, pp. 398-405, 2016.

47. S. B. Wang, F. F. Wang, Z. M. Su, X. N. Wang, Y. C. Han, L. Zhang, J. Xiang, W. Du and N. Tang, "Controllable Fabrication of Heterogeneous p-TiO2 QDs@g-C3N4 p-n Junction for Efficient Photocatalysis," *Catalysts*, vol. 9, no. 5, pp. 15, 2019.

48. X. Wang, R. Xia, E. Muhire, S. B. Jiang, X. J. Huo and M. Z. Gao, "Highly enhanced photocatalytic performance of TiO2 nanosheets through constructing TiO2/TiO2 quantum dots homojunction," *Applied Surface Science*, vol. 459, pp. 9-15, 2018.

Peer-reviewed version available at *Nanomaterials* **2019**, *9*, 1628; doi:10.3390/nano9111628

Table of Contents Graphic: